Design of a Microfluidic Device to Measure the Deformability of Cancer Cells

Gabriel R. López Marcial
Mechanical Engineering, University of Puerto Rico at Mayaguez

NNIN REU Site: Cornell NanoScale Science and Technology Facility, Cornell University, Ithaca, NY
NNIN REU Principal Investigator: Jan Lammerding, Biomedical Engineering, Cornell University
NNIN REU Mentor: Patricia Davidson, Weill Institute for Biomolecular Engineering, Cornell University
Contact: gabriel.lopez3@upr.edu, jan.lammerding@cornell.edu, patricia.davidson@cornell.edu

Abstract and Background:

Metastasis is defined as a "tumor growth or deposit that has spread via lymph or blood to a body area remote from the primary tumor in a cancer patient" [1]. To spread in this manner, cancer cells must deform and pass through dense tissues or blood vessels with constrictions as small as a few microns. Understanding how these metastatic cells deform may give researchers valuable information to diagnose or treat cancerous patients.

The project goal was to create a polydimethylsiloxane (PDMS) microfluidic device that enables the perfusion of cancer cells through narrow constrictions while imaging the cells on a microscope. The well-defined constrictions would force the cell to deform its usually stiff and large nucleus and permit its mechanical characterization. We expect metastatic cells to be more deformable and to transit through the constrictions faster than non-metastatic cells.

The device design was generated using AutoCAD software and transferred to a wafer by photolithography with spin-coated SU-8 photoresist. The wafer was then used as a mold for the final PDMS channels. The cells entered the device through an inlet and were perfused through multiple 5 × 10 μm constrictions. The efficiency of the device is currently being evaluated using images acquired by high-speed video microscopy.

Microfluidic devices for studying nuclear mechanics are not new. However, previous perfusion devices presented problems that greatly impeded their success. In these predecessors, clustering of cells, accumulation of debris and other large particles frequently clogged the main channels of the microfluidic device containing the constrictions.

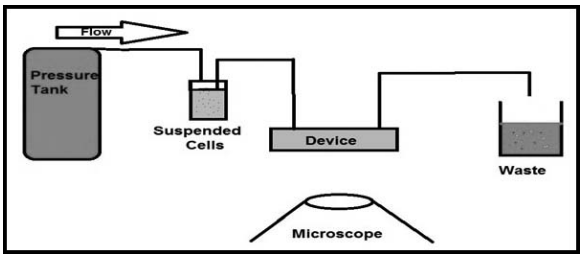

Figure 1: Schematic of perfusion experiments. A gas cylinder pressurizes the air in a tube with the cell suspension, pushing cells through the device at a constant pressure. The device is imaged using a microscope equipped with a high speed camera.

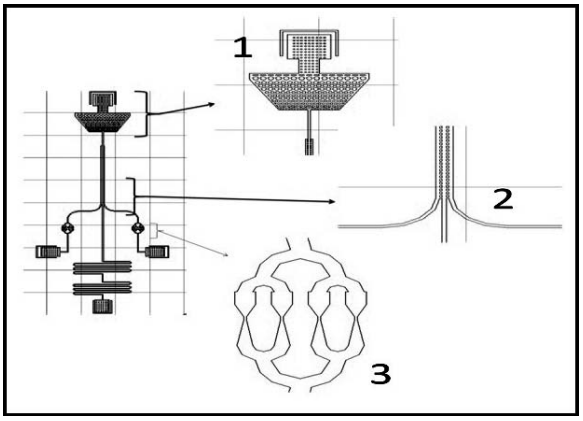

Figure 2: Innovations to the perfusion device design. Seventeen different devices were created with variations in cross-flow filter length, size of constrictions or shape of pillars in cross-flow channel.

Methods:

Devices were designed using AutoCAD software. These patterns were then transferred to a silicon wafer spin coated with SU-8 photoresist using photolithography. The PDMS was poured over the wafer, cured, peeled off, and bound to a glass slide to create the actual experimental device [2]. Perfusion experiments were performed to test the functionality of the devices. Cells in suspension were pushed through the device by a constant pressure of 10 psi. A schematic of the perfusion experiment is shown in Figure 1.

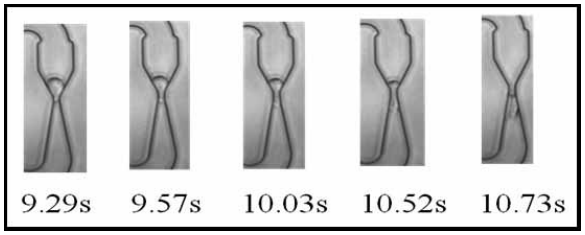

Figure 3: Cell passing through a single constriction in the perfusion device. Below each frame is the time stamp from the video, in seconds. As seen in this example, most cells pass through the 5 x 10 µm constrictions very quickly, making the high speed imaging a necessity for data analysis.

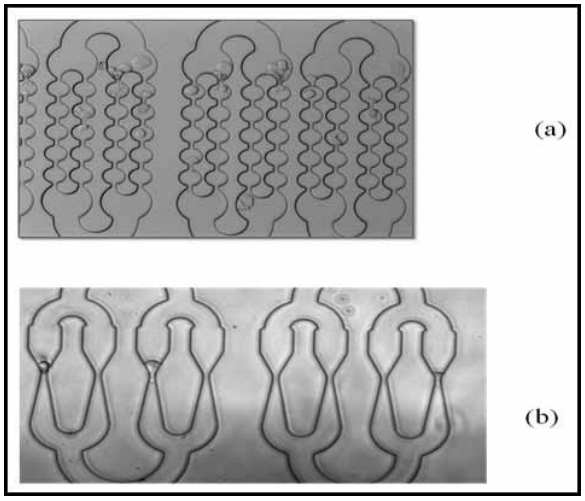

Figure 4: Device comparison. (a) The previous perfusion device, where larger particles and accumulation of cells block the main channels. (b) The new device, which only shows clogging in the far left channel, but is otherwise better suited for perfusion experiments.

Results:

Our new device design (Figure 2) features; (1) an improved coarse filter to hold back debris and larger cells, (2) a cross-flow filter [3] whose purpose is to sort the cells and keep them in a single file to prevent clustering of multiple cells, and (3) redesigned funnel shaped constrictions, through which the cells must deform. A wafer with 17 different variations of this new device was made. The devices varied in small details such as length and width of the cross-flow filter, round or square pillars, and the type of constrictions (single funnel, multiple funnels, or bubbles).

Using the same experimental setup as in previous experiments, we observed significantly reduced clogging of the revised microfluidic device. While devices based on the previous design typically became clogged within a minute or two of the start of the experiment, the new devices performed for periods of 30 to 60 minutes without the constriction channels becoming blocked, allowing for more time to collect experimental data.

After perfusion experiments, an average of 53% of cells were routed into the side constriction channels. Out of these channels, less than 20% of the channels became clogged at any given time. This is a significant improvement over previous designs that exhibited clogging in more than 50% of the channels. Based on preliminary observations, the different variations in length or shape of cross-flow filter had no discernible effect on cell sorting or prevention of blocked channels.

Conclusions:

The new device exhibits reduced clogging and more sustained throughput during the perfusion experiments. Future work will analyze the deformation of the cell nucleus when passing through the constrictions of these perfusion devices in metastatic and non-metastatic cancer cells.

Acknowledgements:

I thank the Cornell NanoScale Facility at Cornell University for giving me the opportunity to be an REU intern this summer, and Jan Lammerding for the great dynamic in his laboratory. I would also like to thank everyone in the Lammerding Lab, especially Patricia Davidson and Celine Denais, for always being there to teach me and help me. Thanks also go out to the National Nanotechnology Infrastructure Network Research Experience for Undergraduates (NNIN REU) Program, the National Science Foundation, and the Department of Defense Breast Cancer Idea Award [BC102152] for providing funds for our work, as well as to Melanie-Claire Mallison and Rob Ilic, the program coordinators at CNF. Everyone played a huge role in my work and is uniquely appreciated.

References:

[1] Dorland, William. 2007. Dorland's Medical Dictionary for Health Consumers. Saunders, an imprint of Elsiever, Inc.

[2] Isermann, P., Davidson, P.M., Sliz, J.D., and Lammerding, J. Assays to measure nuclear mechanics in interphase cells. Curr Protoc Cell Biol. 2012 Sep; Chapter 22: Unit22.16. 2012.

[3] Ji, H., Samper, V., Chen, Y., Heng, C., Lim, T., and Yobas, L. Silicon based microfilters for cell separation. Biomed devices, Springer, 2007.

Designing Directional Micro-Machined Microphones

Alexandro Rocha, Jr.
Applied Science in Nanotechnology, Northwest Vista College in San Antonio, Texas

NNIN REU Site: Microelectronics Research Center, The University of Texas, Austin, TX
NNIN REU Principal Investigator: Dr. Neal A. Hall, Electrical and Computer Engineering, University of Texas at Austin
NNIN REU Mentor: Michael Kuntzman, Electrical Engineering, University of Texas at Austin
Contact: ajrocha2009@gmail.com, nahall@mail.utexas.edu, mlkuntzman@gmail.com

Abstract:

The newest smart phone designs, using noise rejection algorithms, rely strongly on high signal-to-noise ratio (SNR) audio capture. Techniques currently used, involve measuring the difference signal between two "standard" omnidirectional microphones physically separated in space. However, the ability to resolve small difference signals is limited by poor matching or high noise microphones. We designed a pivoting micro-machined microphones that measure spatial pressure differences directly, therefore two microphones are no longer required, reducing cost, power consumption, size, and eliminating microphone matching issues. We found that the rocking structure of the device, anchored by pivots, naturally senses pressure gradients, making it potentially more sensitive than the standard two-omnidirectional-microphone techniques being used. When designing and simulating devices using AutoCAD and ANSYS, we obtained a figure of merit of the first modal resonance showing optimization near the center of the audio band, between (1-3 kHz) to ensure the highest sensitivity and good directivity over the desired range of operation. We discovered that designs that are more flexible will move more in response to an excitation force and have a higher voltage output per input acoustic pressure. During the designing process, we saw that devices with a thinner epitaxial layer and/or thinner and longer pivots produce better figures of merit allowing for lower minimal detectable signal.

Introduction:

The purpose of this project was to design a new directional micro-machined microphone based on a previous design that would provide a lower minimal detectable signal (MDS). The MDS is one of the most important measures of fidelity of a microphone. It is the lowest possible signal that a device can read at the noise floor of the sensor and low MDS is critical for good audio quality and modern noise cancellation features. Figure 1 shows the original design of the in-plane directional microphone with a micrograph inset on the anchored pivot region [1]. It shows the spring component on the outside edge of the device. This was removed in the new device to enhance flexibility.

Experimental Procedure:

We first looked at Hooke's law, $F = kx$, where "k" is the stiffness coefficient. From this formula, we determined that designs that are less stiff will move more in response to a given excitation force and will produce higher voltage output per Pascal of acoustic pressure, and therefore will be more sensitive. We want this in order to produce a low MDS. We used Microsoft Excel to calculate the MDS along with two other figures of merit: 1st modal resonance frequency and capacitance. The 1st modal resonance is proportional to the square root of k so devices with lower 1st modal resonance will have lower stiffness and higher sensitivity. With all other factors being equal, higher capacitances will relax the design requirements on the readout electronics. We tested independent variables that consisted of the thickness of the epitaxial layer between (4-200 μm), and the length between (50-600 μm) and width between (25-200 μm) of the beam pivots. Figure 2 shows a graph comparing the MDS and the pivot width, which shows to be proportional to each other; therefore we are able to conclude that devices with thinner pivots will produce a smaller MDS.

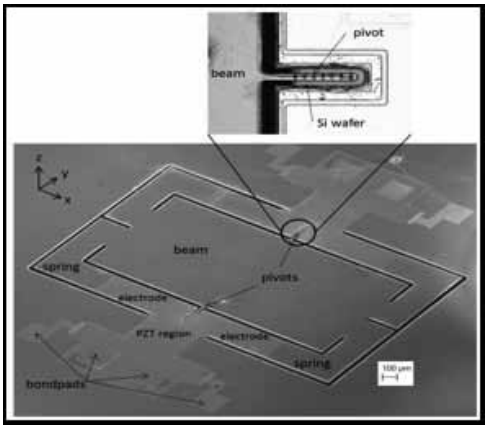

Figure 1: SEM of Generation 1 in-plane microphone with a micrograph inset on the anchored pivot region.

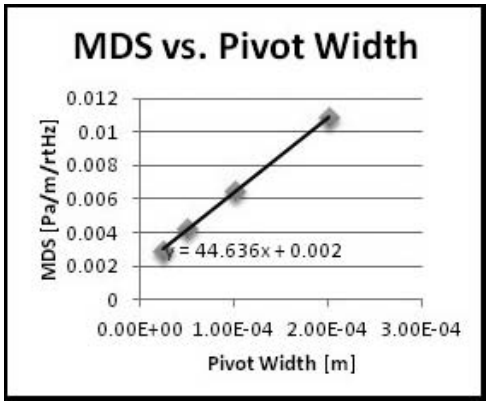

Figure 2: Minimal detectable signal is proportional to pivot width.

We used ANSYS simulation software to find the dependent variables consisting of the 1st and 2nd modal resonance frequencies. Figure 3 shows the ANSYS simulation of the 1st modal resonance frequency of Device A.

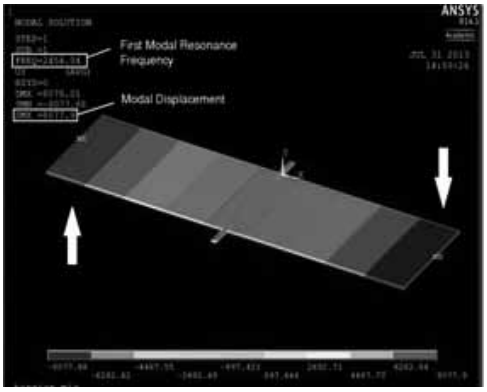

Figure 3: First mode of directional microphone excites from opposite forces pushing from opposite directions.

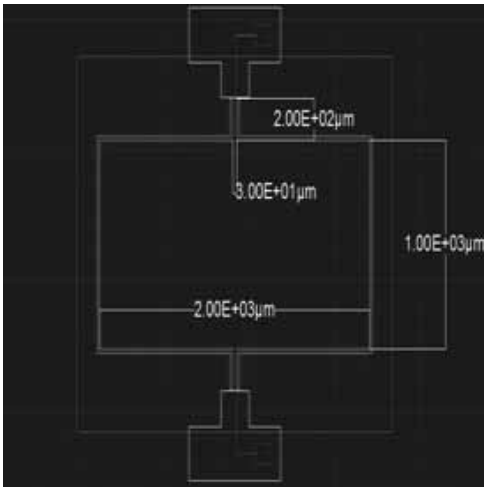

Figure 4: AutoCAD layout of Design B.

Results and Conclusions:

The final steps in the designing process were to decide on four devices that could be fabricated with high quality. We then used AutoCAD, which is a drafting software used to create mask files for fabrication. We decided on using a standard epitaxial layer thickness of 10 μm with all four designs, however alterations were made in the following designs:

Design A; a 50 μm pivot width and a 200 μm pivot length.

Design B; a 30 μm pivot width and a 200 μm pivot length.

Design C; a 25 μm pivot width and a 100 μm pivot length.

Design D; a 50 μm pivot width and a 300 μm pivot length.

We designed the masks in five layers: Top electrodes, bottom electrodes, backside etching, device layer, and lead zirconate titanate (PZT) layer, which is the piezoelectric material being used in the device. Figure 4 shows the AutoCAD mask layout of Design B with all five layers included. The final masks were successfully designed and are awaiting delivery for fabrication.

Future Work:

There is still much to accomplish in order to complete the project with fabrication and characterization of the final devices being the main finishing points. Given the high sensitivity of our mechanical structure combined with the low dielectric loss of our piezoelectric material, the device can result in much more efficient MDS than the current state of the art microphone with regard to pressure gradient measurements. The designs could have an immediate impact on the noise rejection capabilities of next generation smart phones.

Acknowledgements:

I would like to give my sincere gratitude to the National Nanotechnology Infrastructure Network Research Experience for Undergraduates (NNIN REU) Program and National Science Foundation for the opportunity to gain experience in the nanotechnology research field. Also, thank you to my principal investigator Dr. Neal Hall, mentor Michael Kuntzman, site coordinator Dr. Marylene Palard, the University of Texas at Austin, and all of the faculty and staff that provided an extravagant working environment for the ten week program. Finally, I thank Dr. Qiaoying Zhou from Northwest Vista College for always encouraging me to pursue my goals.

References:

[1] M.L. Kuntzman, J. Glorial Lee, N.N. Hewa-Kasakarage, D. Kim, N.A. Hall, Micro-machined piezoelectric microphones with in-plane directivity, Applied Physics Letters (2013) 054109.

Studying the Interfacial Dynamics of Miscible Systems with Microfluidics

John Schwalbe
Chemical and Biomolecular Engineering, Cornell University

NNIN REU Site: NanoTech User Facility, University of Washington, Seattle, WA
NNIN REU Principal Investigator: Dr. Amy Q. Shen, Mechanical Engineering, University of Washington
NNIN REU Mentor: Shilpa Beesabathuni, Mechanical Engineering, University of Washington
Contact: jas699@cornell.edu, amyshen@uw.edu, shilpanb@uw.edu

Abstract:

Various microfluidic features are considered for the study of the interfacial dynamics of miscible systems. We take advantage of upper critical solubility temperature (UCST) behavior of a given miscible system. Fully realizing the potential of our experimental plan will require integrating multiple features in one microdevice. The challenges that arise include varying length scales between features, temperature control, and complex control systems.

Introduction:

We are interested in the dynamics of interfaces between two miscible phases. While interfaces between equilibrated phases are thermodynamically stable, interfaces between miscible phases are inherently transient. These interfaces exhibit interesting mass transfer properties and effective interfacial tension [1]. Understanding these dynamics is important to modeling various industrial and biological processes. Enhanced oil extraction and mucus spreading in the lungs are two examples. Droplet microfluidics is an ideal platform to study interfaces because the small length scales allow for very controlled velocity profiles.

The devices were fabricated using soft lithography [2], so they could be prototyped quickly.

To observe the dynamics of miscible interfaces, it was important that we have a known initial condition. To do this, we took advantage of the temperature dependence of solubility. Below a critical temperature, the UCST, two immiscible phases form. Above it, the two components are miscible in all proportions. To exploit this experimentally, droplets were formed below the UCST, denoted as phases I and II in Figure 1. Next, a single droplet was trapped above a heater. The droplet was then heated above the UCST, shown with dot-dash lines in Figure 1. Finally, thermodynamics took over and the droplet began to dissolve, shown with dashed lines in Figure 1. Isobutyric acid (IBA) and water have a reasonable UCST, for example. But, there are other interesting systems that could be explored with this technique including ionic liquids and thermoresponsive polymers. Implementing this plan was difficult. Droplet formation, trapping, and heating on a single chip were all challenging.

Experimental Procedure:

We considered a variety of device features. For droplet formation, we used T-junctions and flow-focusers [3]. In a T-junction, a channel carrying the dispersed phase entered a channel carrying the continuous phase at 90°. Depending on the relative sizes of the channels and the flow rates, T-junctions

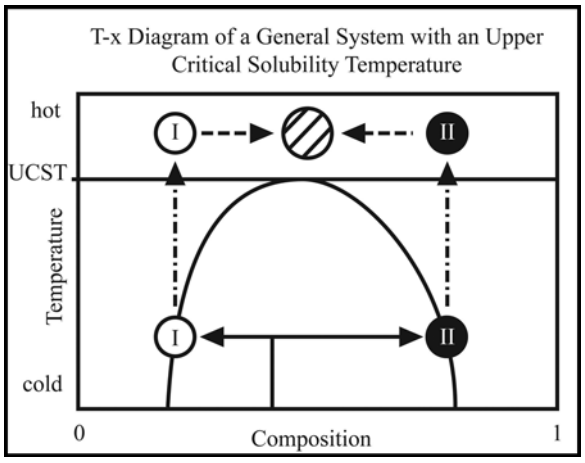

Figure 1: Process schematic.

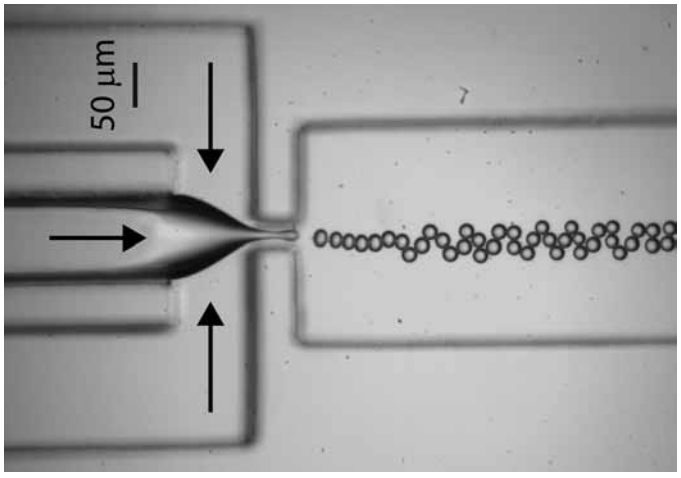

Figure 2: A flow focuser producing droplets of water in oil.

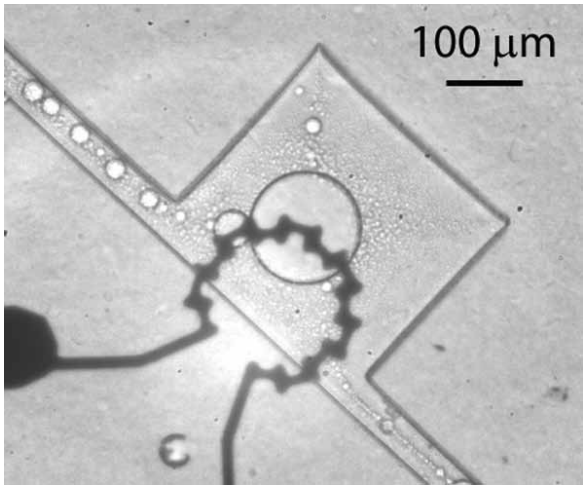

Figure 3: An IBA/water emulsion in a vortex trap.

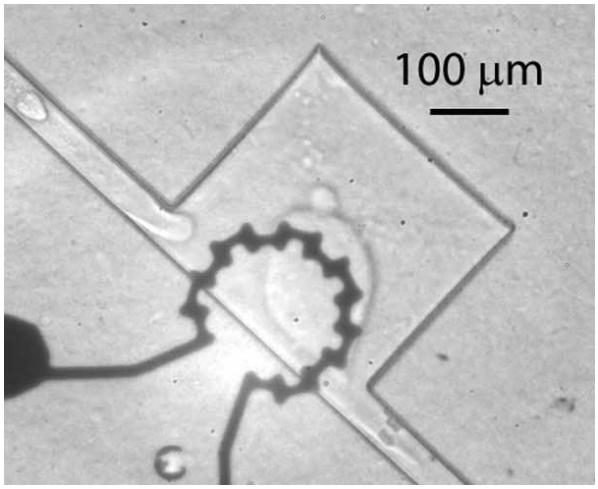

Figure 4: An IBA/water mixture shortly after it was heated above the UCST.

could generate droplets of varying sizes in either a dripping or a jetting mode. In a flow-focuser, the dispersed phase was introduced into the middle of the carrier phase. The resulting two-phase flow was then forced through a constriction. The resulting viscous and capillary forces caused the dispersed phase to break into droplets, as seen in Figure 2 [3].

Trapping the droplet was the next challenge. Cross-slot chambers were a powerful option. They consisted of two channels crossing at 90°. In use, the channels acted as two inlets and two outlets. This created a stagnation point in the middle of the chamber where a droplet could be trapped. When used in conjunction with a feedback control system, droplets could be trapped indefinitely [4]. Another attractive feature was that the droplet deformed in the velocity field, and the effective surface tension could be deduced from the shape of the droplet [5].

A hydrodynamically simpler option was a vortex trap. An emulsion in a vortex trap can be seen in Figure 3. At high enough flow rates, a vortex will form in the expansion. Vortex traps have been used to trap cells [6]. But, it is an open question whether or not they can also be used to trap droplets.

Finally, temperature control was vital to this experiment. Traditional thermal stages cannot ramp the temperature fast enough. We chose resistance heaters made with a lift-off procedure instead. The geometry of the heater could be tweaked to get the desired performance. But, electrolytic gas production was observed in some designs above a threshold voltage. So, it is a constrained optimization problem.

Results and Discussion:

A fully integrated device remains elusive. The most successful feature was the heater. Figure 4 shows the result of heating an emulsion above the UCST of the system, in this case IBA and water. The blurring of the interface clearly shows the dissolution process and the shape of the droplet reflects the effective interfacial tension. However, the variations along the circumference of the droplet show the need for a more homogenous temperature increase. This image also highlights the need for an integrated device. The small droplets surrounding the central droplet are undesirable. They are there because an emulsion was pumped into the trap rather than the uniform droplets that a flow-focuser or T-junction would create.

But, as Figure 3 shows, the vortex traps have potential. Their simplicity is an inherent advantage. They require no complicated feedback control. However, viscous droplets cannot cross streamlines in the sense that particles can. So far vortex traps have worked with emulsions, but this may pose a problem with the orderly, monodisperse droplets produced by a T-Junction or a flow-focuser.

Acknowledgements:

I would like to thank Professor Boris Stoeber and Vahid Bazargan from the University of British Columbia for the fabrication of certain devices. I would also like to thank the UW MFF staff for their invaluable assistance and training. I would like to thank the entire Shen lab for helping me at every opportunity, and the National Nanotechnology Infrastructure Network Research Experience for Undergraduates (NNIN REU) Program for funding.

References:

[1] Lacaze, Laurent, et al. Physical Review E 82, 041606, 1-8. 2010.

[2] Xia, Y., and Whitesides, G. Annu. Rev. Mater. Sci. 28:153-84. 1998.

[3] Christopher, G, and Anna, S. J., Phys. D: Appl. Phys. 40, R319-R336 (2007).

[4] Melikhan Tanyeri, et al., Lab Chip, 11, 1786-1794, 2011.

[5] Cabral, Joao, and Hudson, Steven. Lab Chip, 6, 427-436, 2006.

[6] Soojung Claire Hur, et al., Biomicrofluidics 5, 022206 1-10. (2011).

Full-Body Silicon Medical Tweezers for Cancerous Tissue Detection and Characterization

Connie Wu
Electrical Engineering and Finance, University of Pennsylvania

NNIN REU Site: Cornell NanoScale Science and Technology Facility, Cornell University, Ithaca, NY
NNIN REU Principal Investigator: Prof. Amit Lal, Electrical and Computer Engineering, Cornell University
NNIN REU Mentor: Po-Cheng Chen, Electrical and Computer Engineering, Cornell University
Contact: wuconnie@seas.upenn.edu, amit.lal@cornell.edu, pc445@cornell.edu

Abstract:

We designed and created the first prototype of a full-body silicon surgical tool for detecting and characterizing cancerous tissue. From literature, it had been shown that tissue elasticity and electrical permittivity have been promising non-optical markers for identifying cancerous tissue [1]. Because of the advantages of micro-fabrication technology, a full body silicon device in a tweezer structure was designed and employed with numerous sensors. Strain gauges were used for tissue elasticity by monitoring the insertion force, and the platinum wires were designed for tissue permittivity measurements. Additionally, the platinum electrodes have the capability of electrical physiology signal measurements. Strain gauge resistivity measurements were performed to verify the performance of the tweezers and feasibility for future medical applications.

Introduction:

If a surgeon were to staple bad tissue into the affected site during a colon anastomosis, there is a high chance of intestinal leakage and subsequent high risk for the patient. Our goal is to design a medical tool that can help surgeons distinguish abnormal tissue from normal tissue. The full body silicon tweezer with several different sensors on it can provide assistance for the doctor during operation. The tweezer structure is easily accessible to surgeons, and since the body is constructed from a continuous piece of silicon, it allows for flexibility in integrating sensors and CMOS circuitry for more function, such as wireless transmission of measured signal.

Experimental Procedure and Process:

The device structure was designed using L-Edit and Matlab code that can automatically generate Caltech Intermediate Format (CIF) files with parameter alteration capability. The structural parameters included the hinge radius, hinge thickness, leg length, leg thickness, hinge beginning angle, hinge ending angle, and inter-probe distance.

The first prototype design had a hinge radius of 8000 μm, leg length of 4 cm, thickness at the hinge of 400 μm, and leg thickness of 1000 μm. The tweezers were laser cut for structural testing, during which it was verified the tweezers inter-probe distance could deform at least 5000 μm.

In a COMSOL simulation, it was found that the point of maximum stress at 80.7 MPa was at the apex of the hinge, while the normal stress fracture of silicon was around 1-3 GPa. Four probes were placed on each leg of the tweezers and finger holders were placed along the mid-section of the legs. Each probe had a Wheatstone bridge strain gauge at the cantilever junction. In the eight probes, the strain gauges resistors were realized with LPCVD polysilicon implanted with boron at a dose of 2×10^{15} ions/cm^2 at 100 keV. The sheet resistance of polysilicon was ~ 185 ohms/$\square$. The resistors were electrically contacted with aluminum alloy (Al + 1% silicon) metal lines. Insulating PECVD nitride was deposited, followed by platinum evaporation to define electrical recording sites and permittivity sensors. The device layers are depicted in Figure 1.

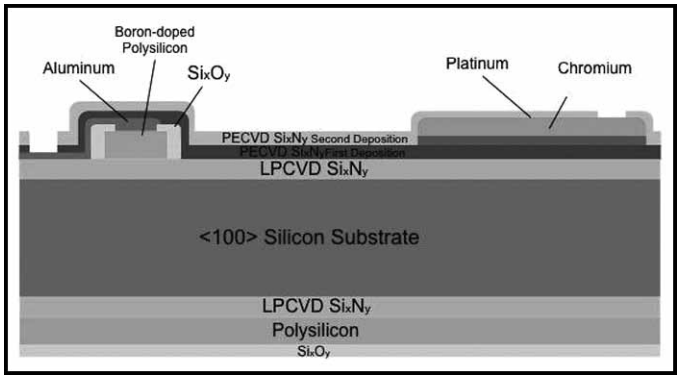

Figure 1: Fabrication layers of the tweezers.

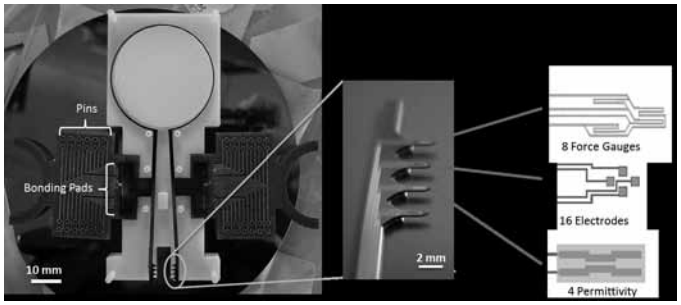

Figure 2: Assembled tweezer device with holder.

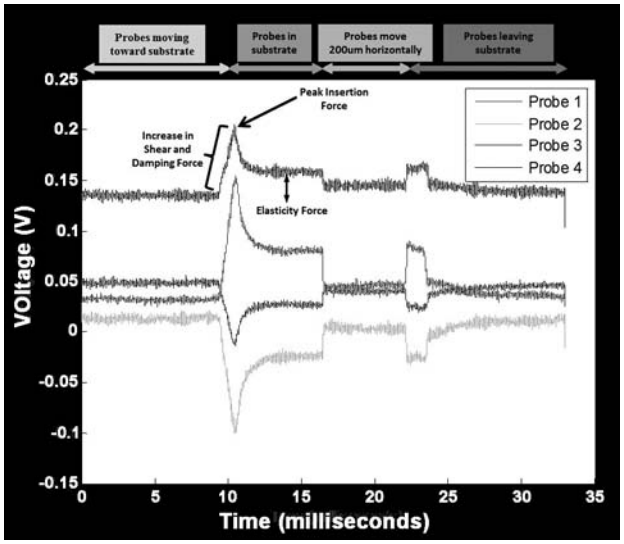

Figure 3: Probe force gauge output at 3000 µm/s insertion speed with horizontal movement of 200 µm.

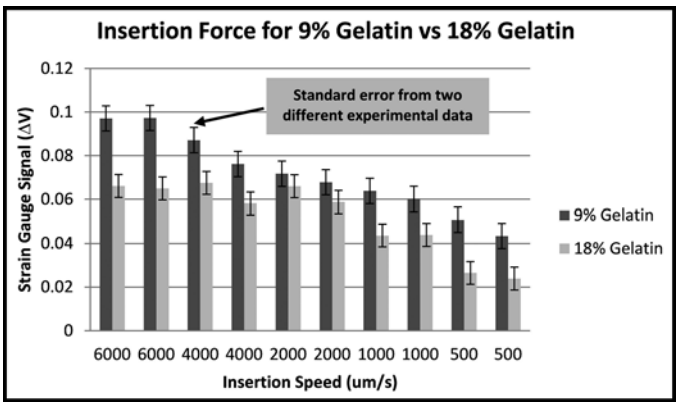

Figure 4: Probe signal from gelatin concentration change.

All of the sensors were connected to the 56 bonding pads located in the finger holders (Figure 2). These bonding pads were wired to a PCB board with pins for testing. The strain gauge pins were connected to a differential amplifier with a gain of 200 that transmitted probe voltage signals to LabView.

Results and Conclusions:

The full body silicon medical tweezers included eight strain gauges, four sets of platinum wires and sixteen platinum electrodes (Figure 2). To test the spring constant of the tweezers, one leg of the tweezers was fixed while the other was displaced horizontally. COMSOL estimated that the spring constant would be around 2 N/m while the empirical result yielded a spring constant was 9 N/m. To test the strain gauge signals, four probes were positioned 8608 μm vertically above 6% gelatin mixture and preset to a 6000 μm/s insertion speed for the control experiment. To get the insertion force signal, we calculated the difference between the signal levels from before the probe is inserted into the gelatin and after it penetrates the sample surface (Figure 3).

Four parameters were altered: insertion speed, insertion height, insertion direction, and gelatin concentration. The results from the experiments indicated that insertion force increased with insertion speed by ~ 15% for every 1000 μm/s increase in speed. Insertion height was found to be negligible when insertion speed was controlled. Whereas the insertion direction in which the substrate was normal to the force gauge had a larger signal change than when the probe tip was normal to the substrate.

An increase of gelatin concentration from 9% to 18% decreased the insertion force by an average of 28% (Figure 4). The strain gauge data profile showed some promising indicators for tissue properties such as a peak for initial insertion force, a second level of height for the tissue elasticity force, and a low reading for when the probe had left the tissue.

Future Work:

Next, we will create a case for the tweezers so that the structure can be durable during surgical usage. Furthermore, more tests will be conducted on healthy tissue versus cancerous tissue to better characterize the force gauge readings. Also, to more comprehensively characterize the tissue samples, the electrodes and capacitors will also be tested and calibrated for usage.

Acknowledgments:

I would like to thank my principal investigator, Amit Lal, and my mentor, Po-Cheng Chen, for providing the inspiration for this project. I am also thankful to the NNIN REU Progam and NSF. Lastly, I would like to thank the CNF staff for fabrication assistance.

References:

[1] K. Yan. "A real-time prostate cancer detection technique using needle insertion force and patient-specific criteria during percutaneous intervention." Medical Physics v. 36, Issue 9 (2009).

[2] P.-C. Chen. "Ultrasonic Neural Probe for Real Time Electromechanical Histology of Neural Interfaces," (Hilton Head 2012).